https://doi.org/10.1016/j.cemconres.2021.106565

Effect of seawater as mixing water on the hydration behaviour of tricalcium aluminate

Yamei Cai [a], Dongxing Xuan [a], Pengkun Hou [b], Jie Shi [b], Chi Sun Poon [a,*]

[a] Department of Civil and Environmental Engineering, The Hong Kong Polytechnic University, Hong Kong

[b] Shandong Provincial Key Lab for the Preparation and Measurement of Building Materials, University of Jinan, Jinan, Shandong, China

Abstract: This study explored the mechanism of the effect of seawater on tricalcium aluminate (C_3A) hydration. The results showed that seawater retarded C_3A hydration and reduced the reaction degree of C_3A. The co-existence or ion pairing of Ca^{2+} and SO_4^{2-} onto the surface of C_3A poisoning the reactive sites is the main reason for this retardation. Besides, the precipitation of $Mg(OH)_2$ on the surface of C_3A would prolong the induction period for another 30 minutes and then consequently decrease the dissolution rate of C_3A hydration. Trace amounts of $MgSO_4^0$ and Mg^{2+} present in the alkaline solution had little retardation effect. It was also found that Cl^- would preferentially react with C_3A to form Friedel's salt, rather than forming hydroxy-AFm as that in the C_3A-deionized water paste. The direct formation of Friedel's salt resulted in an accumulation of Al^{3+} in solution, which would also hinder the subsequent dissolution of C_3A.

Keywords: Seawater; C_3A; retardation; hydration; Friedel's salt.

1. Introduction

In Portland cement, tricalcium aluminate (C_3A), as the most reactive phase, affects the setting time, workability and rheological property of fresh cement or concrete [1], even though

it only accounts for approximately 5-10 % by mass of ordinary Portland cement. It has been well acknowledged that the reaction rate of C_3A with water is extremely rapid leading to the precipitation of calcium hydroaluminates. This would lead to flash set [2]. To avoid this phenomenon, gypsum is always incorporated into Portland cement clinkers during the grinding process to delay the hydration.

With respect to the retarding mechanism of gypsum (sulphates) on the C_3A hydration, the physical barrier effect mainly caused by the precipitation of ettringite (AFt) on the C_3A surface has been questioned [3]. Geng et al. [4] reported that the needle network of AFt at the dissolution front of C_3A was highly porous, which was not possible to act as a dense barrier layer. In comparison, more and more researchers support the adsorption mechanism. It has been pointed out that the initial reactivity of C_3A was reduced through SO_4^{2-} alone adsorbed onto the active sites of C_3A surface [5-7] or through Ca^{2+} and SO_4^{2-} adsorbed on an aluminium-rich layer that was formed on the surface of C_3A due to its partially dissolution [8-10]. However, Myers et al [11, 12] put forward that the adsorption behaviour of SO_4^{2-} on the surface of C_3A was not supported by the geochemical literature, because little or no adsorption of SO_4^{2-} onto Al (hydr)oxides above pH 7-10. Therefore, they proposed that the ion pairing of $CaSO_4^0$ would adsorb on this aluminium-rich layer, which would decrease the local undersaturation of Ca^{2+} in aqueous solution near C_3A surface sites and consequently retard the C_3A dissolution. However, in contrast to the adsorption mechanism of Ca^{2+} and/or SO_4^{2-}, Joseph et al. [13] suggested that the precipitation of AFt on the surface of C_3A could also block the active sites of C_3A. This process would be consistent with a dissolution-controlled mechanism [10], rather than a diffusion-controlled mechanism which is the case for the coating mechanism of AFt. Referring to these studies above, the retarding mechanism on the initial dissolution of C_3A still need to be further explored.

Meanwhile, it was also reported that the type of sulphates would determine the delaying effect on the C_3A hydration. When the amount of SO_4^{2-} was the same, $MgSO_4$ had the greatest retardation effect on the hydration of C_3A, followed by $CaSO_4$ and Na_2SO_4 [14]. For this phenomenon, it can be inferred that the adsorption of SO_4^{2-} alone on the surface of C_3A is not the sole reason for retarding the hydration of C_3A. The cation-specific effect was proposed to explain it [15, 16]. As for the retarding mechanism of $MgSO_4$ on C_3A hydration, a simple extension from $CaSO_4$ to $MgSO_4$, i.e., the adsorption of Mg^{2+}, SO_4^{2-} or $MgSO_4^0$ onto the reactive sites of C_3A to inhibit its initial dissolution, was proposed, considering many of the comparable chemical properties between Ca^{2+} and Mg^{2+} [14, 15]. Moreover, it was also reported that, when C_3A was mixed with $MgSO_4$, there was a lower ratio of Ca/Al and a higher ratio of Mg/Ca on the surface of C_3A particles [16], implying that Mg^{2+} would partially substitute for Ca^{2+} in the near surface crystal structure due to a higher affinity on the C_3A surface and a relatively smaller ionic radii [16, 17]. The replace of Ca^{2+} by Mg^{2+} would contribute to a relatively longer induction period. Based on the above disputation, the magnesium species present in alkaline environments should be clarified at first, then the role of different magnesium species on C_3A hydration needs to be further analysed.

Currently, the possible use of seawater for concrete production has gained increasing interest [18-22]. In the above reviewed studies, the effect of sulphate alone on the hydration of C_3A was emphasized. In comparison, seawater is a complex system, containing different cations and anions. The specific ions in seawater that are responsible for inhibiting the hydration of C_3A are still unclear. The purpose of this study is thus to fill the research gap, understand the interaction between the C_3A and seawater and further explore how these interactions influence the initial dissolution and hydration evolution of C_3A. This work would provide new insights on the role of seawater in regulating the C_3A hydration process.

However, it has been shown that the C_3A exhibits polymorphism, which depends on the alkali contents and is also influenced by the cooling rate during the production process of cement [23-25]. In cement clinkers, cubic C_3A and orthorhombic C_3A usually exist alone or in combination [23]. The different crystal structure of C_3A can influence its reactivity. It has been reported by Boikova et al. [26] that, in the absence of sulphates, orthorhombic C_3A was less reactive than cubic C_3A. However, when sulphate was present, the hydration of orthorhombic C_3A was faster than that of the cubic C_3A [27, 28]. But, as reported in the literatures [29-35], the relative amount of cubic C_3A to orthorhombic C_3A in Portland cements indicates that the cubic C_3A is usually the dominant phase in most commercial cements. Therefore, this study focused on the hydration behaviour of the cubic C_3A when hydrating in seawater. Isothermal Calorimetry, XRD, SEM, ICP-OES and Ion Chromatography were carried out to characterize the development of cubic C_3A hydration using deionized water (DI) and simulated seawater (SW) respectively as the mixing water. Thermodynamic modelling software (GEMS) was further used to simulate the evolution of equilibrium phases and the change of solution chemistry of seawater under different pH conditions.

2. Materials and experimental methods

2.1 Materials

A synthesized cubic tricalcium aluminate (C_3A) in powder form (provided by DMT Materials Technology Company in Shanghai of China) was used in this study. The specific surface area of C_3A measured by N_2 adsorption and desorption was 611.9 m^2/kg, and its particle size distribution and morphology are shown in Fig. 1, indicating that its median particle diameter was 13.7 μm and its shape was angular. The QXRD result in Fig. 2 shows that the purity of C_3A was higher than 95 %, and the free lime and mayenite ($C_{12}A_7$) contents were about 0.04 % and 4.30 %, respectively.

According to ASTM D1141-98 [36], a simulated seawater was prepared and its chemical composition and main ionic concentration are shown in Table 1. 0.1 N NaOH solution was used to adjust the pH value of seawater to 8.2. All chemicals used in this work were analytical grades.

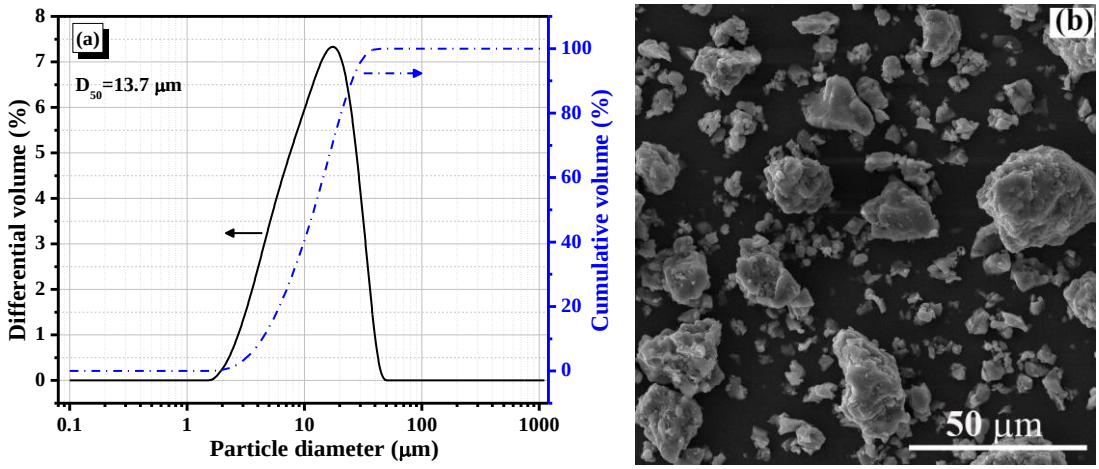

Fig. 1 The particle size distribution and morphology of C_3A

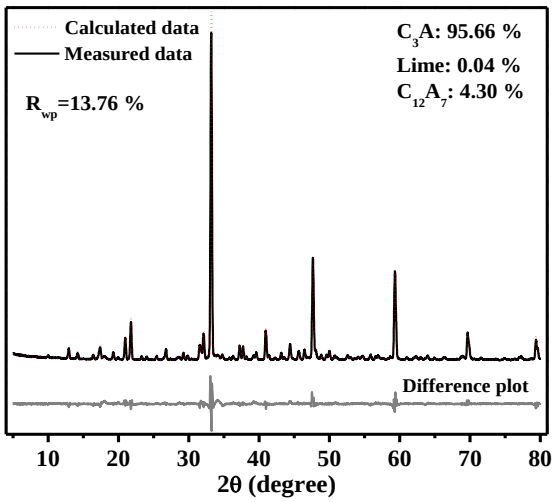

Fig. 2 XRD of C_3A by Rietveld refinement

Table 1. Chemical composition and main ionic concentration of simulated seawater [36]

Chemicals	Concentration (g/L)	Ions	Ionic concentration (g/L)
NaCl	24.530	Na^+	11.020

$MgCl_2$	5.200	Mg^{2+}	1.326
Na_2SO_4	4.090	Ca^{2+}	0.418
$CaCl_2$	1.160	K^+	0.400
KCl	0.695	Cl^-	19.830
$NaHCO_3$	0.201	SO_4^{2-}	2.765
KBr	0.101	HCO_3^-	0.146
H_3BO_3	0.027	Br^-	0.068
$SrCl_2$	0.025	Sr^{2+}	0.014
NaF	0.003	-	-

2.2 Sample preparation

In this work, DI and SW were used to prepare C_3A pastes using a water-to-solid ratio of 1.0. At first, the C_3A powder and DI or SW were placed in 50 mL centrifugal tubes, and then these samples were vigorously agitated in a vortex apparatus for 1 min. After the required reaction durations from 2 min to 12 h, the liquid was collected after centrifugation at 10000 rpm for 5 min and passing through a 0.45 μm membrane filter. Then the filtrated liquid samples were stored in a fridge at 5 ± 1 ^oC prior to testing. Additionally, the solid residues remained in the tubes were immediately immersed in liquid nitrogen for about 15 min. Then the frozen samples were transferred to a freeze-dryer for drying for another 5 h. Once dried, the samples without grinding were stored in a desiccator until further testing.

2.3 Experimental techniques

2.3.1 Isothermal calorimetry

The hydration heat evolution of C_3A mixed with DI or SW was monitored using a TAM Air isothermal calorimeter at 20 ^oC until 3 days. The water-to-solid ratio of C_3A pastes was set to 1.0. In this work, internal mixing method was used for experimental groups contained C_3A-DI paste, because the initial process (0-10 min) of hydration was studied due to the extremely rapid hydration reaction of C_3A-DI paste. 2 g C_3A powder was placed in a glass ampoule, and 2 g solution was introduced into a syringe. After the solution was injected, the paste was stirred

by a mechanical rotor for 2 min. However, the internal mixing intensity was set to a very low speed to prevent the disturbance or damage of calorimeter [37]. When the early process was not of interest (<10 min), external mixing was preferred [37]. Thus, when comparing the length of induction period and major exothermic peak of C_3A-SW and C_3A-S2 (S2 denotes seawater solution excluded $MgCl_2$), the external mixing method was used to prepare the pastes by hand stirring using a glass rod for 2 min, and the sample was quickly introduced into the calorimeter (less than 5 min after mixing).

2.3.2 Ion chromatography

The concentrations of Cl^- and SO_4^{2-} in the collected liquid in Section 2.2 were measured using ion chromatography (Dionex AS-DV, Thermo Scientific). At different reaction periods, the filtrates collected were diluted using Milli-Q water prior to testing.

2.3.3 ICP-OES

The concentrations of cations in the collected filtrates, i.e., Ca^{2+}, Al^{3+}, Mg^{2+}, were characterized by an inductively coupled plasma/optical emission spectroscopy (ICP-OES, FMX36, SPECTROBLUE). Before measurement, the liquid samples extracted from C_3A and SW or DI mixes in Section 2.2 were digested with concentrated nitric acid and then diluted with 5% nitric acid.

2.3.4 X-ray diffraction (XRD)

In order to follow the evolution of hydration products at early ages, in-situ XRD measurements were conducted. After mixing with SW or DI for 1 min, the fresh C_3A paste was directly casted in the XRD sample holder. A Kapton film was used to cover the C_3A paste to prevent the loss of water and carbonation during the test. The XRD (Rigaku SmartLab 9kW-

Advance) measurement was carried out in a 2θ range of 5 ^{o} to 36 ^{o} with a step width of 0.02 ^{o}, and the scan speed was fixed at 30 ^{o}/min. During measurement, CuKα was used as radiation source.

Due to the fast scanning speed and the contribution of the Kapton film and water in the sample, it was not possible to quantify the absolute amounts of various phases. The freeze-dried samples in Section 2.2 were co-ground with corundum (10 wt.%), and the quantitative X-ray Diffraction (QXRD) technique with internal standard was used to characterize the amount of unhydrated C_3A in different periods. The samples were scanned from 5^{o} to 60^{o} at a speed of 2.5 ^{o}/min with a 0.02^{o} increment.

2.3.5 Scanning electron microscopy (SEM)

The morphology of the hydration products in the C_3A-DI/SW paste was observed by a scanning electron microscope equipped with an energy dispersive X-ray detector (SEM, TESCAN VEGA3). This equipment was operated at ~0.001 Pa and in secondary electron mode at a 20 kV voltage, a 60 μA beam current and a working distance of ~10 mm. After drying, the unground solid residues collected in Section 2.2 were stuck on carbon tape attached on SEM sample holders. These samples were gold coated before observation.

2.3.6 GEMS modelling

By using the PSI-Nagra database [38] and the Cemdata 18 database [39-41], a thermodynamic modelling software (GEMS) was used to assess the variation of solution chemistry of seawater under different pH conditions and the evolution of equilibrium phases in the C_3A-SW paste. For modelling the development of equilibrium phases in the C_3A-SW system, firstly, the reaction degree of C_3A in the C_3A-SW paste at different reaction time was obtained using QXRD as mentioned in Section 2.3.4. Then, a four-parameter logistic non-linear

regression model (4PL) was used to fit data points of C_3A dissolution degree [42, 43]. After that, this fitting curve, i.e., the dissolution degree as a function of time, was used as kinetic input for GEMS [42].

3. Results and discussion

3.1 Influence of seawater on C_3A hydration

3.1.1 Hydration heat evolution of C_3A

Fig. 3 shows the hydration heat evolution of C_3A mixed with DI and SW. For the C_3A-DI paste and the C_3A-SW paste, the main exothermic peak appeared at 3.8 min and 1.7 h, respectively, indicating that a delay of hydration of C_3A was caused by seawater. When comparing the two exothermic peaks, i.e., Q_1 and Q_2, Q_2 was lower and broadened with a relatively smaller rising slope, which demonstrated a relatively slower hydration reaction when C_3A was mixed with SW.

For the cumulative heat release in Fig. 3 (b), there was a lesser amount of heat release in the C_3A-SW paste than that in the C_3A-DI paste, i.e. the corresponding heat release was decreased by 24% at 72 h. In addition, the curve of the C_3A-SW paste reached a stable value at about 30 h, while the corresponding time for C_3A-DI paste was about 72 h. These features indicated a relatively lower reaction degree when C_3A was mixed with SW.

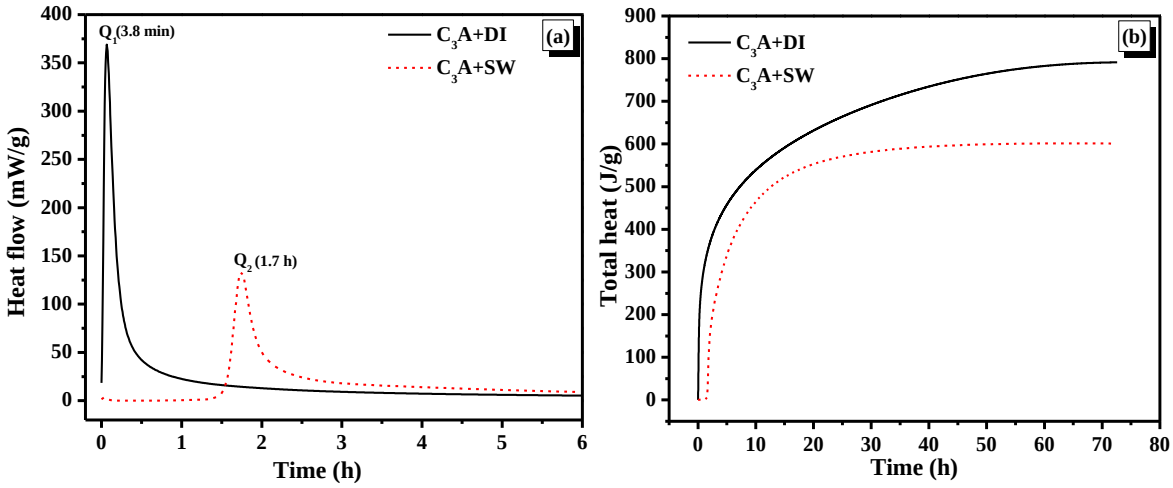

Fig. 3 Development of hydration heat of C_3A mixed with DI and SW

3.1.2 Hydration products of C_3A

Fig. 4 shows the in-situ XRD patterns of the C_3A pastes mixed with DI and SW. It can be noticed that the reaction of C_3A with DI was extremely rapid. From Fig. 4 (a), plenty of C_4AH_{13} and C_2AH_8 (hydroxy-AFm) were detected after just 9 minutes. With the increase in hydration time, the intensity of C_4AH_{13} and C_2AH_8 peaks increased, indicating the continuous hydration reaction of C_3A. In the first 12 h, the metastable C_4AH_{13} and C_2AH_8 phases were the major hydration products, even though the stable C_3AH_6 phase was also detected and its intensity slightly increased with hydration time.

In comparison, when SW was used as the mixing water shown in Fig. 4 (b), during the first 30 min, no crystalline hydrates were detected by XRD. This was due to the retardation effect of seawater on the C_3A hydration as mentioned above. After 1.5 h, a peak at about 11° (2 θ) was obviously observed, indicating the formation of Friedel's salt ($Ca_4Al_2Cl_2(OH)_{12}\cdot 4H_2O$). At 4 h, the peak of C_3AH_6 was also observed, and its amount increased with time. However, the metastable C_4AH_{13} and C_2AH_8 were no longer detected, revealing that, compared to OH^-, the Cl^- in seawater could preferentially react with C_3A to form Friedel's salt.

In order to compare the hydration degree of C_3A in DI and SW, the amount of the hydrated C_3A was calculated from QXRD data and the results are tabulated in Table 2. It was found that, at 30 min and 1 h, only 0.6 % and 12.7 % of C_3A were reacted when SW was used as the mixing water, while 52.0 % and 54.8 % of C_3A were consumed for the case of using DI. At 3 d, the reaction degree of C_3A in SW was still 8.2 % lower than that in DI. These results reflected that the use of seawater would delay the hydration reaction of C_3A and decrease its reaction degree.

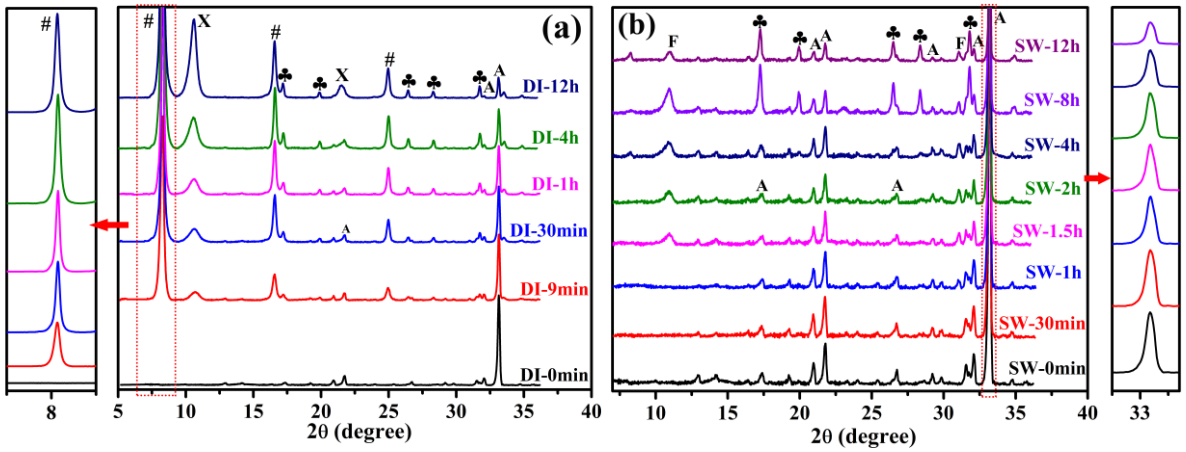

Fig. 4 In-situ XRD patterns of C_3A mixed with DI or SW for different times ((a): C_3A-DI system, (b): C_3A-SW system). A: C_3A (tricalcium aluminate); #: C_2AH_8 (calcium hydroaluminate); X: C_4AH_{13} (calcium hydroaluminate); ♣: C_3AH_6 (hydrogarnet); F: Friedel's salt;

Table 2 Hydration degree of C_3A in C_3A-DI/SW pastes as calculated by QXRD

Items / Ages	Hydration degree of C_3A (%)	
	C_3A+DI	C_3A+SW
30 min	52.0	0.6
1 h	54.8	12.7
4 h	59.9	44.5
8 h	73.5	61.0
12 h	75.1	62.9
3 d	94.5	86.3

Fig. 5 presents the morphology evolution of hydration products in the C_3A-DI/SW paste. For the C_3A-DI paste in Fig. 5 (b) and 5 (c), after hydrating for 5 min and 2 h, the formed calcium hydroaluminates were flaky, and most of them were stacked up. In contrast, when SW was mixed with C_3A for 30 min in Fig, 5 (d), the C_3A particle still had a relatively smooth surface, indicating less reaction. At 2 h, the hydration products with a honeycomb shape precipitated on the C_3A surface. These hydrates should be Friedel's salts, because their characteristic peaks were detected by XRD as shown in Fig. 4 (b). The arrangement of the

Friedel's salt was disordered, unlike its assemblage reported in some literatures [44-46]. According to Talero [47], a relatively slow precipitation rate of the Friedel's salt would perhaps lead to a more-ordered hexagonal shape. Thus, the precipitation rate of the Friedel's salt in the C_3A-SW paste could be quicker than that in other reported situations, such as OPC system. Furthermore, after 12 h of hydration, the paste prepared with SW had a similar morphology to that of the C_3A-DI system in Fig. 5 (c), as a high amount of cubic C_3AH_6 was formed.

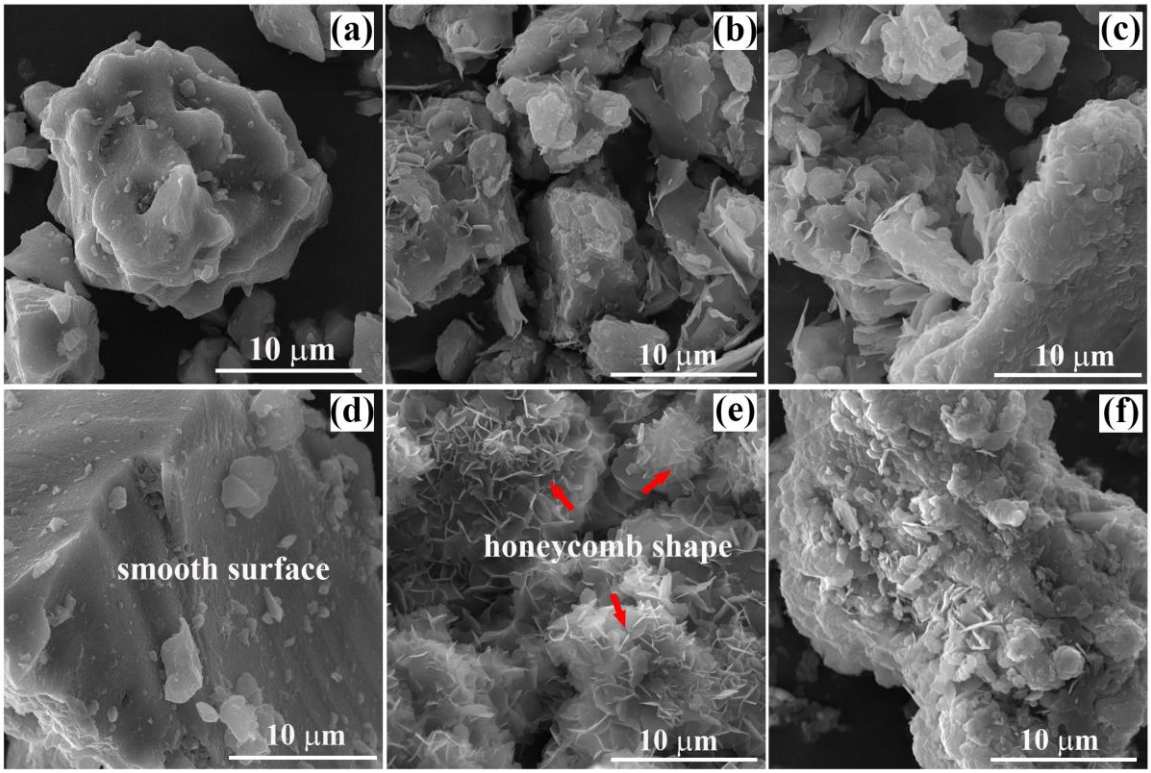

Fig. 5 Morphology of hydrates in the C_3A-DI/SW paste at different times ((a): pure C_3A (b): C_3A+DI-5 min, (c): C_3A+DI-2h, (d): C_3A+SW-30 min , (e): C_3A+SW-2 h, (f): C_3A+SW-12 h)

3.1.3 Variation of ionic concentrations during C_3A hydration

Fig. 6 displays the change of concentrations of different ions as a function of time in the C_3A-DI/SW paste. The ionic concentrations at time zero denoted the corresponding concentration in the pure simulated seawater and DI water, respectively.

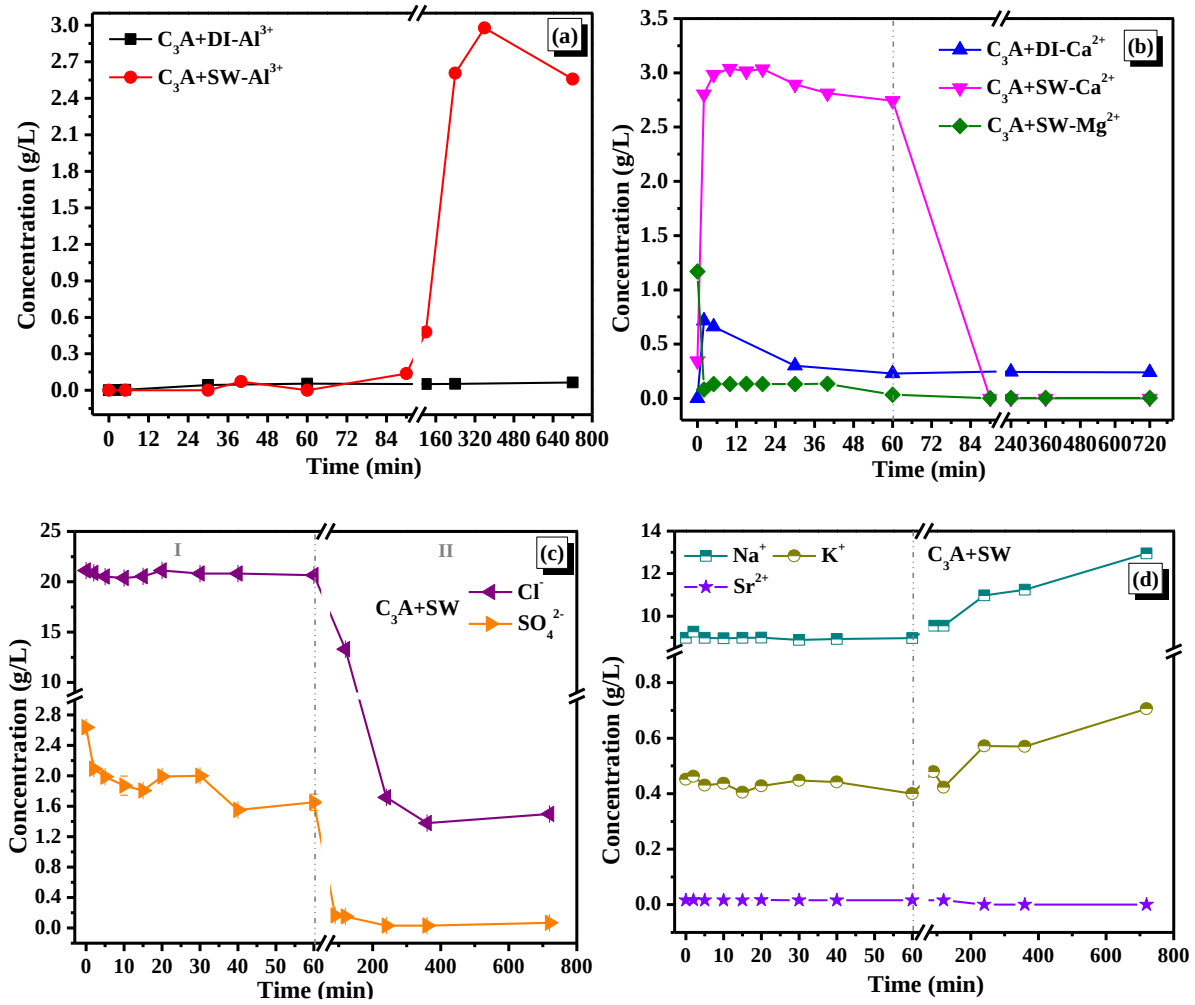

Fig. 6 Different ionic concentrations as a function of hydration time in the C_3A-DI/SW paste

Fig. 6 (a) shows when C_3A was mixed with DI, little Al^{3+} concentration was detected in the solution, as almost all of the dissolved ions immediately precipitated to form calcium hydroaluminates due to the rapid hydration reaction depicted in Figs. 3 and 4 (a). In comparison, when C_3A was mixed with SW, within the first hour, a low concentration of Al^{3+} were observed due to the lower initial reactivity of C_3A during the induction period. But after 1.5 h, a high concentration of Al^{3+} was found in the solution, which corresponded to the initial formation stage of Friedel's salt in Fig. 4 (b). This implied that, unlike the formation of calcium hydroaluminates (C_4AH_{13} and C_2AH_8) in the C_3A-DI paste, the formation of Friedel's salt in the C_3A-SW paste would result in an accumulation of Al^{3+} in the solution. The specific reason will be further discussed in Section 4.2. After 6 h, the concentration of Al^{3+} began to decrease,

and at the same time a noticeably increased XRD peak intensity of C_3AH_6 appeared at 8 h as shown in Fig. 4 (b), implying an increased amount of C_3AH_6 formed in this period.

Compared with Al^{3+}, a relatively high concentration of Ca^{2+} was released from C_3A, especially during the initial contact with DI or SW [15]. From Fig. 6 (b), the concentration of Ca^{2+} in the C_3A-SW paste at 2 min was 4 times higher than that of the C_3A-DI paste. This could be explained by an accelerated initial dissolution of C_3A as shown in Equation (3-1) due to the consumption of OH^- by Mg^{2+} to precipitate $Mg(OH)_2$. Fig. 6 (b) shows a decrease of Mg^{2+} concentration by 93% at 2 min. After 1 h, the decrease in the concentration of Ca^{2+} might be due to the formation of Friedel's salt and hydroaluminates caused by further hydration of C_3A.

$$Ca_3Al_2O_6 + 6\,H_2O \rightarrow 3\,Ca^{2+} + 2\,Al(OH)_4^- + 4\,OH^- \quad (3\text{-}1)$$

For the Mg^{2+}, from SEM images in Fig. 7, it can be observed that some magnesium compounds were attached on the surface of C_3A after 5 min and 30 min of hydration, which could be due to the precipitation of $Mg(OH)_2$. The influence of magnesium species on the C_3A hydration will be further discussed in Section 3.2.2 and 4.1.

Furthermore, in the case of C_3A mixed with SW, the concentration changes of Cl^-, SO_4^{2-}, Na^+, K^+ and Sr^{2+} introduced by seawater are shown in Fig. 6 (c) and 6 (d). For Cl^-, before 1 h, it decreased by only 2%. But after 1 h, the consumption of Cl^- was caused by the reaction between Cl^- and C_3A to form the Friedel's salt as revealed by XRD pattern in Fig. 4 (b). After 6 h, the concentration of Cl^- became stabilised, while the amount of C_3AH_6 was significantly increased (Fig. 4 (b)), indicating the formation of C_3AH_6 after the Friedel's salt.

Regarding the concentration of SO_4^{2-}, during the first 1 h, its concentration deceased by 37%. Together with the modest decrease of Ca^{2+} during the first 1 h, this could be due to the adsorption of Ca^{2+} and SO_4^{2-} on the surface of C_3A, which resulted in the retardation of C_3A hydration [6, 10, 11, 14]. After 1 h, the concentration of SO_4^{2-} significantly dropped to close to zero, but no related new products were detected from XRD. The reason might be that a small

amount of SO_4^{2-} in the C_3A-SW paste, i.e., only about 0.3 wt. % of the mass of C_3A, was incorporated in the hydration products, like the Friedel's salt or C_3AH_6 phase. The specific reason still needs to be further explored.

With respect to the evolution of other cations shown in Fig. 6 (d), the concentration of Na^+, K^+ and Sr^{2+} remained stable in the first 1 h of hydration, indicating that these cations in seawater were neither adsorbed on the C_3A surface nor substituted Ca^{2+} that had been adsorbed on the C_3A surface to retard its hydration. After 1 h, the concentrations of Na^+ and K^+ slightly increased owing to the depletion of free water due to C_3A hydration.

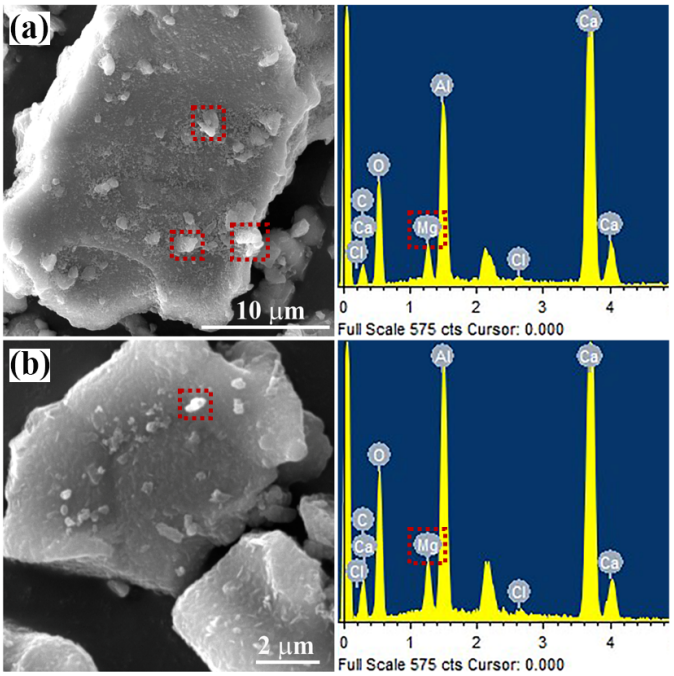

Fig. 7 SEM and EDS results of C_3A mixed with SW for 5 min (a) and 30min (b)

3.2 Role of SO_4^{2-} and Mg^{2+} in seawater on C_3A hydration

3.2.1 Effect of SO_4^{2-}

Many literatures have reported the retardation effect of SO_4^{2-} on C_3A hydration when gypsum or other forms of sulphate alone was present [9, 13, 14, 16]. In order to further confirm the role of SO_4^{2-} in seawater on the C_3A hydration, the sulphate salt was selectively excluded when preparing the seawater for this part of the study, and the corresponding change of heat

evolution of the C_3A paste (C_3A-S1) is shown in Fig. 8. Compared with the original C_3A-SW paste, when the SO_4^{2-} was removed (C_3A-S1), there was no induction period in the heat evolution curve. This indicated that SO_4^{2-} in seawater had a determinative effect on the occurrence of the induction period. Comparing with the C_3A-DI paste, after the removal of SO_4^{2-} from the seawater, the occurrence of the major heat evolution peak was accelerated by about 3 min. This could be due to the slight acceleration effect derived from the reaction of C_3A and Cl^- in seawater. To further demonstrate this effect, a NaCl solution with the same concentration in the simulated seawater was mixed with C_3A, the similar accelerating effect for the heat flow curve further validated the action of Cl^- in Fig. 8.

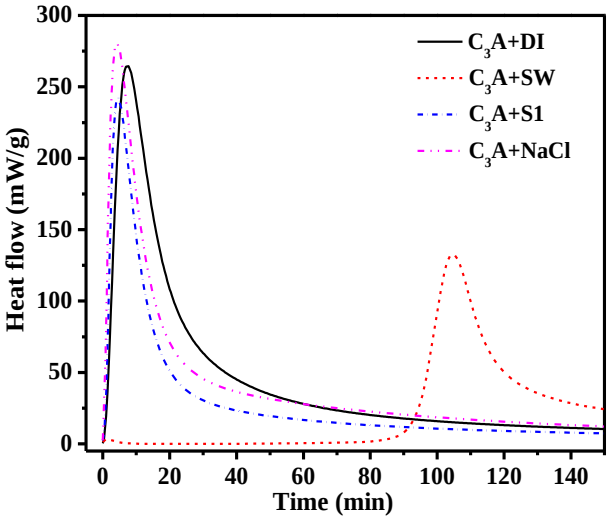

Fig. 8 Effect of SO_4^{2-} in seawater on the hydration rate of C_3A. The solution name of S1 in the specimen of C_3A+S1 denotes the simulated seawater without Na_2SO_4.

3.2.2 Effect of Mg^{2+}

In order to explore the effect of Mg^{2+} in seawater on the C_3A hydration, a seawater solution without adding the magnesium salt (S2) was used to prepare the C_3A paste, and its evolution of hydration heat is shown as plotted by the red dashed line in Fig. 9. In contrast, the corresponding change in the heat flow of C_3A mixed with the original seawater (C_3A-SW) is

shown as the black line in Fig. 9. It was found that when Mg^{2+} was not involved into the seawater (C_3A-S2), the induction period was shortened by approximately 30 minutes. It can be deduced that the Mg^{2+} in seawater would contribute to the hydration retardation of C_3A as well. In the Section 4.1, the possible reasons will be further discussed.

Furthermore, the slope of the hydration heat curve of the C_3A-S2 paste in both the acceleration and deceleration periods were steeper than that in the C_3A-SW paste. In addition, the peak intensity of the C_3A-S2 paste was also higher than that of the C_3A-SW paste. This could be inferred that, in the C_3A-SW paste, the presence of Mg^{2+} in seawater would decrease the dissolution rate of C_3A and the formation rate of hydration products, which will be further discussed in Section 4.1.

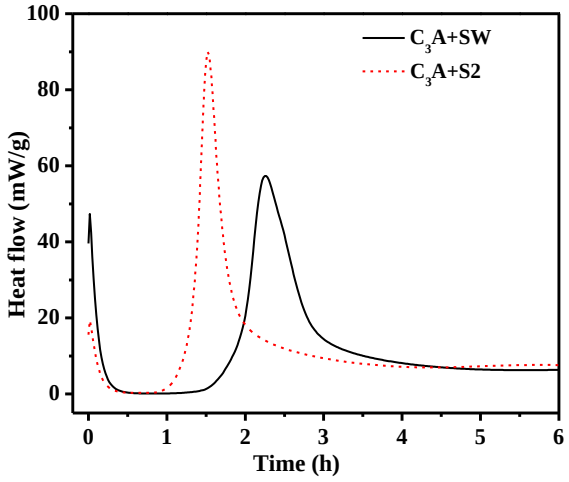

Fig. 9 Effect of Mg^{2+} on the hydration rate of C_3A. The solution name of S2 in the specimen of C_3A+S2 denotes the simulated seawater without $MgCl_2$. (Note: An external mixing method was adopted in this test. The initial peak could thus be affected due to the disturbance of moving samples into the calorimeter. This peak was not analysed in the work.)

4. Discussion

4.1 Effect of seawater on the C_3A hydration process

As illustrated in Fig. 3, seawater had a retardation effect on the C_3A hydration. After excluding SO_4^{2-} in seawater (Fig. 8), this retardation phenomenon disappeared. This demonstrated that the critical and determinative role of SO_4^{2-} in seawater on the retarded hydration of C_3A, even though the amount of SO_4^{2-} in this system only accounted for 0.3 wt. % of the mass of C_3A.

In order to further scrutinize the chemical form of SO_4^{2-} in seawater, GEMS (Gibbs Energy Minimization Software) was used to simulate the concentration variation of sulphate species in seawater under different pH conditions, and the results are illustrated in Fig. 10 (a). It was found that, when C_3A contacts with seawater, the leaching of Ca^{2+} and OH^- would increase the pH value in this system. In this case, the amount of ion pairing of $CaSO_4^0$ in this system was increased to about 4.7 mmol/L. Thus, the complexation of the ion pairing of $CaSO_4^0$ in the solution onto the Al-rich leached layer of C_3A could poison the reactive sites and retard its hydration reaction. This theory has been experimentally supported by other researchers who explored the hydration behaviour of C_3A with sulphates [12, 15]. In addition, another possible reason could be that the Ca^{2+} is first chemisorbed onto the Al-rich leached layer of C_3A, forming a positive charge, and then the negatively charged SO_4^{2-} would be adsorbed on the surface [9]. Therefore, the adsorption of $CaSO_4^0$ or the successive adsorption of Ca^{2+} and SO_4^{2-} on the Al-rich layer of C_3A would explain the retarding effect of seawater on the C_3A hydration. Moreover, no AFt was detected in this low concentration of SO_4^{2-} in Fig. 4. In this case, the retardation phenomenon could mainly derive from the adsorption of the above ions or ion pairing, rather than the adsorption of AFt onto the active sites of C_3A [13]. This further confirms the important role of the adsorption of Ca^{2+} and SO_4^{2-} or $CaSO_4^0$ on C_3A surface in retarding the C_3A hydration.

However, it has been acknowledged that seawater contains more than one kind of cation. In this case, except for the role of Ca^{2+} and SO_4^{2-}, the interaction of Mg^{2+} and SO_4^{2-} is another concern. The thermodynamic tendency of Mg^{2+} species in seawater with the increase of pH value is also presented in Fig. 10. The initial pH value in the Figs. 10 (a) and 10 (b) was that of the simulated seawater at 8.2. From these two figures, it can be found that, pH value would increase due to the dissolution of C_3A, consequently the amount of ion pairing of $MgSO_4^0$ and Mg^{2+} reach zero due to the precipitation of $Mg(OH)_2$. Besides, the evolution of magnesium species in the pore solution of C_3A-SW paste in the first 5 min of hydration was further simulated using GEMS and shown in Fig. 10 (c). The decrease of Mg^{2+} and $MgSO_4^0$ and the increase of $Mg(OH)_2$ (s) were obvious, and at about 1.5 min, the concentration of $MgSO_4^0$ was close to zero. The experimental data shown in Fig. 6 (b) in the Section of 3.1.3 also showed a reduction of the concentration of Mg^{2+} by 93% at only 2 min of hydration, which was in agreement with the simulation result in Fig. 10 (c). Therefore, the adsorption of $MgSO_4^0$ or the successive adsorption of Mg^{2+} and SO_4^{2-} on the Al-rich layer of C_3A that has been reported in the C_3A mixed with single magnesium salt in the solution (e.g. $MaSO_4$) [14, 15] had little effect on the retarded hydration of C_3A under this alkaline environment.

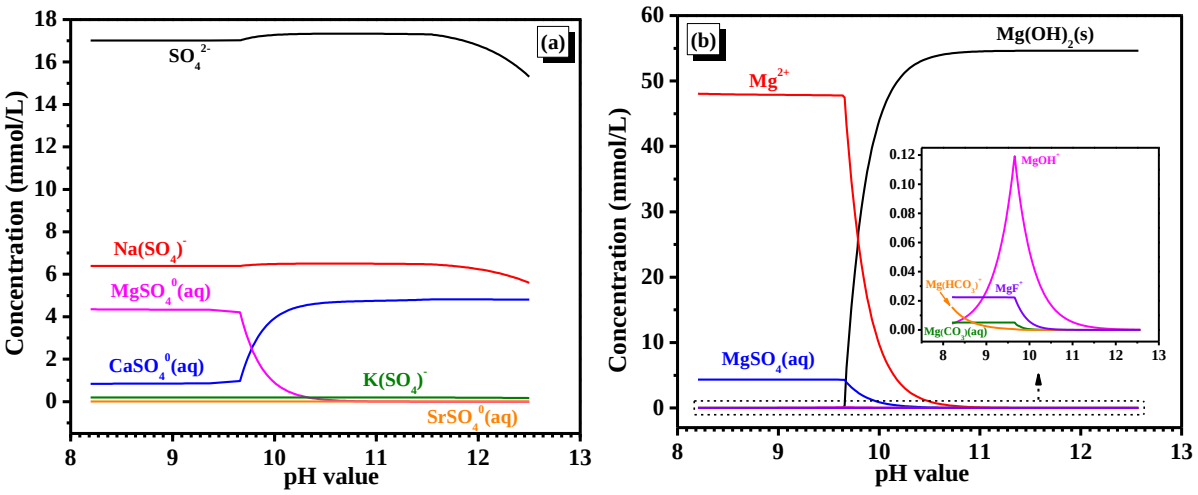

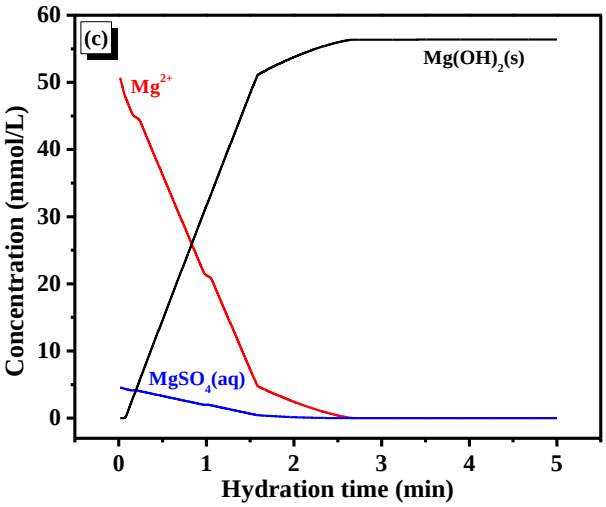

Fig. 10 Variation of sulphate species (a) and magnesium species (b) in seawater under different pH conditions ($Ca(OH)_2$ as the pH regulator). (c): the change of main magnesium species in C_3A-SW system with the increase of hydration time

Furthermore, it was also found that when magnesium salt was removed from the seawater, the induction period was shortened for about 30 minutes (Fig. 9). This also demonstrated that the presence of the magnesium salt also played a role on the retardation effect. But in Fig. 10 (c), it was found that the amounts of $MgSO_4^0$ and Mg^{2+} were decreased to nearly zero at 1.5 min and 2.5 min of hydration, respectively. Therefore, the effects of $MgSO_4^0$ and Mg^{2+} would become insignificant. Considering that $Mg(OH)_2$(s) was the major species after 3 min of hydration as shown in Fig. 10 (c), the precipitation of $Mg(OH)_2$ on the C_3A surface could also block parts of the active sites of C_3A surface to extend the induction period, but its significance was less than the adsorption effect of Ca^{2+} and SO_4^{2-}. Besides, the attachment of $Mg(OH)_2$ on the C_3A surface would to some extent decrease the dissolution rate of C_3A in both the acceleration and deceleration period as shown in Fig. 9.

Compared with Ca^{2+} and Mg^{2+} ions, the concentrations of Na^+ and K^+ ions introduced by the seawater remained relatively stable in the solution during the first 1 h of hydration. Therefore, the possibility that these cations combined with SO_4^{2-} to retard C_3A hydration would be small.

Consequently, the effect of seawater on the retardation of C_3A hydration may be summarised by a schematic diagram in Fig. 11. The initial dissolution of C_3A forms an Al-rich layer with negative charge on the surface of C_3A [12]. This would allow 1) Ca^{2+} to preferentially adsorb on the surface of C_3A, and afterwards, SO_4^{2-} in seawater would migrate to the surface, or 2) the ion pairs of $CaSO_4^0$ present in seawater are directly adsorbed on the C_3A surface. These possible adsorption behaviours could poison the reactive sites of the C_3A surface, which would hinder the further dissolution of C_3A. Besides, the precipitation of $Mg(OH)_2$ from seawater onto the surface of C_3A also would to some extent decrease the dissolution of C_3A and prolong the induction period. In contrast, the adsorption of Mg^{2+} and SO_4^{2-} or the ion pairs of $MgSO_4^0$ on the C_3A surface had less effect on retarding the hydration of C_3A due to the transformation of Mg^{2+} and $MgSO_4^0$ to $Mg(OH)_2$(s) under the alkaline environment.

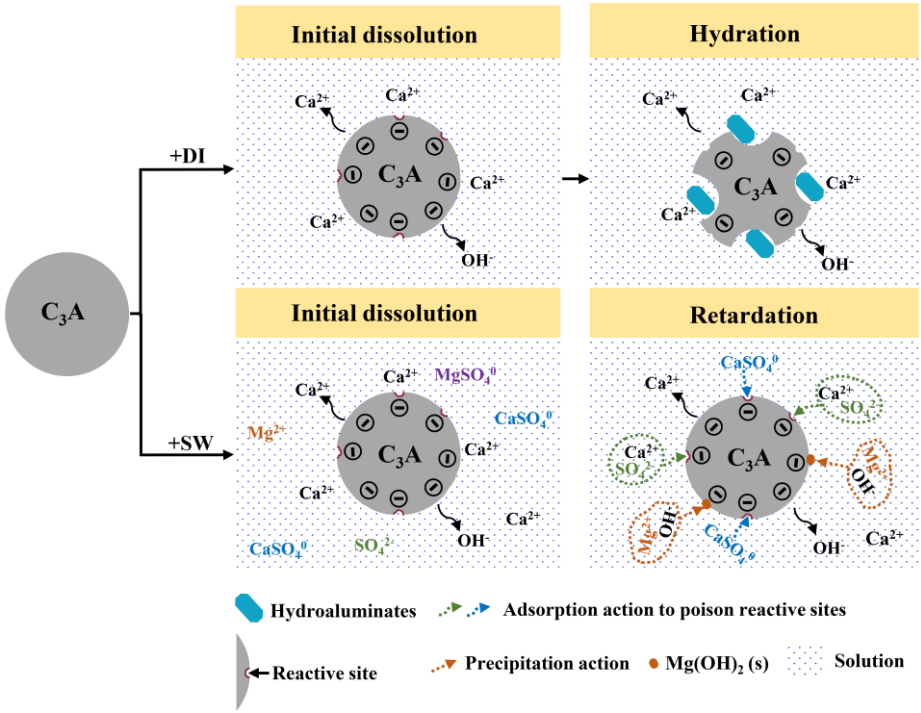

Fig. 11 Schematic diagram of the C_3A hydration and retardation in DI and seawater

After induction period, the concentration of SO_4^{2-} rapidly decreased to close to zero (Fig. 6 (c)), but no related new product was detected as shown in the XRD data (Fig. 4 (b)). This SO_4^{2-} might be adsorbed on the formed hydration products, but this still needs to be further explored.

4.2 Effect of seawater on the hydration products of C_3A

C_3A reacts rapidly with freshwater to form metastable hydroxy-AFm phases (Figs. 3 and 4 (a)), i.e., C_4AH_{13} and C_2AH_8. Finally, these products can be converted to a more stable hydrogarnet phase (C_3AH_6). However, when seawater is mixed with C_3A, after the induction period, the Friedel's salt would be formed first. After that, the amount of C_3AH_6 began to increase (Fig. 4 (b)). The simulated result using the GEMS software in Fig. 12 also confirmed the preferential formation of the Friedel's salt. It was also found that, during this process, no metastable hydroxy-AFm was detected according to the in-situ XRD data (Fig. 4 (b)).

Furthermore, as shown in Eq. (3-1), the molar ratio of Ca^{2+} to $Al(OH)_4^-$ produced by the dissolution of C_3A is 3:2, meaning that the dissolution of 2 mol of C_3A would produce 1 mol of C_4AH_{13} and 1 mol of C_2AH_8 referring as indicated by Eqs. (4-1) and (4-2). Therefore, no significant amount of Al^{3+} was detected in the solution due to the rapid precipitation of C_4AH_{13} and C_2AH_8 in the C_3A-DI paste (Fig. 6 (a)). In contrast, when there is a direct reaction between C_3A and Cl^- to form Friedel's salt in the C_3A-SW paste, according to the molar ratio of Ca^{2+} to $Al(OH)_4^-$ in Equations (3-1) and (4-3), the amount of Ca^{2+} is insufficient. This would result in an accumulation of Al^{3+} and decrease of Ca^{2+} as shown in Figs. 6 (a) and 6 (b). This further illustrates that, when C_3A was mixed with seawater, Cl^- would directly adsorb into the interlayers of the principal layers ($[Ca_2Al(OH)_6]^+$) of AFm structure to form Friedel's salt, rather than forming C_4AH_{13} in which OH^- is replaced by Cl^- through an ion-exchange mechanism [48], because this would not lead to a large amount of Al^{3+} in solution. Besides,

this accumulation of Al^{3+} in solution could also hinder the subsequent dissolution of C_3A, leading to a slower hydration rate of C_3A at the later stage of C_3A-SW paste.

$$4\ Ca^{2+} + 2\ Al(OH)_4^- + 6\ OH^- + 6H_2O \rightarrow Ca_4Al_2(OH)_{14}\cdot 6H_2O\ (C_4AH_{13}) \quad (4\text{-}1)$$

$$2\ Ca^{2+} + 2\ Al(OH)_4^- + 2\ OH^- + 3H_2O \rightarrow Ca_2Al_2(OH)_{10}\cdot 3H_2O\ (C_2AH_8) \quad (4\text{-}2)$$

$$4\ Ca^{2+} + 2\ Al(OH)_4^- + 2Cl^- + 4\ OH^- + 4H_2O \rightarrow Ca_4Al_2Cl_2(OH)_{12}\cdot 4H_2O\ (Friedel's\ salt) \quad (4\text{-}3)$$

Therefore, even though the hydroxy-AFm and Friedel's salt are in the similar calcium aluminium layered double hydroxide (Ca-Al-LDHs) family [2] which is composed of positively charged hydroxide layers ($[Ca_2Al(OH)_6]^+$) and anions, such as OH^-, SO_4^{2-}, CO_3^{2-}, Cl^-, intercalating the interlayer spaces [2, 49-51], when a substantial amount of Cl^- is present in this reaction system, as compared to OH^-, Cl^- would preferentially intercalate the interlayers of $[Ca_2Al(OH)_6]^+$ to form the Friedel's salt. After most of Cl^- is consumed (Fig. 6 (c)), C_3AH_6 starts to form (Fig. 4 (b)), along with a decrease in the concentration of Al^{3+}.

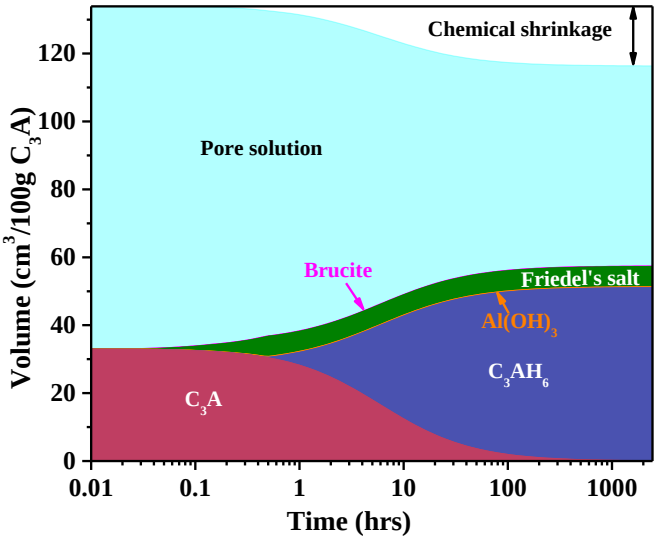

Fig. 12 Modelled evolution of hydration phases at equilibrium in the C_3A-SW paste (Note: The Brucite and $Al(OH)_3$ were not found in XRD data in Fig. 4, which could be due to their relatively small amounts .)

5. Conclusions

This study aims to elucidate the effect of seawater on the cubic C_3A hydration. Isothermal Calorimetry, XRD, SEM, Ion Chromatography and ICP-OES were used to investigate the evolution of hydration heat and hydration products, as compared to that of the C_3A-DI paste. The development of equilibrated hydration phases in the C_3A-SW paste and the variation of ionic species were simulated by GEMS. The following findings can be summarized:

- Using seawater as mixing water retarded the hydration of the cubic C_3A. When SO_4^{2-} was excluded from the seawater, the induction period disappeared. The co-existence or ion pairing of Ca^{2+} and SO_4^{2-} in seawater adsorbed on the surface of C_3A would be the main reason for this retardation.
- Under an alkaline environment, the precipitation of $Mg(OH)_2$ would block parts of the active sites on the surface of C_3A to decrease the dissolution of C_3A and prolong the induction period.
- In the C_3A-SW paste, the Friedel's salt was first detected, followed by C_3AH_6. This was different from the hydration products formed in the C_3A-DI paste, in which the metastable hydroxy-AFm, i.e., C_4AH_{13} and C_2AH_8, were found at the beginning and then they were gradually converted into C_3AH_6. Additionally, the direct formation of Friedel's salt in C_3A-SW paste resulted in an accumulation of Al^{3+} in solution, which would also hinder the subsequent dissolution of C_3A.

As mentioned in the introduction, the crystal structures of C_3A in cement clinker is also an important factor influencing its hydration process. This study mainly focused on the hydration behaviour of the cubic C_3A mixed with seawater, considering that the cubic C_3A is predominant in most Portland cements. However, as the orthorhombic C_3A is also present in some cements, the impact of seawater on its hydration behaviour is worthwhile to be explored. Based on the results of the cubic C_3A mixed with seawater obtained in this work, a possible effect of the

orthorhombic C_3A-seawater paste can be inferred: seawater could retard its hydration, but the degree of retardation could be less than that on the cubic C_3A-seawater paste due to the faster hydration behaviour of the orthorhombic C_3A in presence of sulphate [27, 28]. But the above needs to be further verified.

Acknowledgments

This study work was supported by a grant from the Research Grants Council of the Hong Kong SAR Government (Project No. T22-502/18-R) and The Hong Kong Polytechnic University.

References

[1] M.J. Kim, K.B. Kim, K.Y. Ann, The influence of C3A content in cement on the chloride transport, Advances in Materials Science and Engineering, 2016 (2016) 1-8.
[2] H.F. Taylor, Cement chemistry, Thomas Telford London, 1997.
[3] K.L. Scrivener, P. Pratt, Microstructural studies of the hydration of C 3 A and C 4 AF independently and in cement paste, in: Proc Br Ceram Soc, 1984, pp. 207.
[4] G. Geng, R.J. Myers, Y.-S. Yu, D.A. Shapiro, R. Winarski, P.E. Levitz, D.A.L. Kilcoyne, P.J.M. Monteiro, Synchrotron X-ray nanotomographic and spectromicroscopic study of the tricalcium aluminate hydration in the presence of gypsum, Cement and Concrete Research, 111 (2018) 130-137.
[5] R. Feldman, V.S. Ramachandran, The influence of CaSO4. 2H2O upon the hydration character of 3CaO. Al2O3, Magazine of Concrete Research, 18 (1966) 185-196.
[6] A. Quennoz, K.L. Scrivener, Hydration of C3A–gypsum systems, Cement and Concrete Research, 42 (2012) 1032-1041.
[7] K.L. Scrivener, P. Juilland, P.J. Monteiro, Advances in understanding hydration of Portland cement, Cement and Concrete Research, 78 (2015) 38-56.
[8] M.E. Tadros, W.Y. Jackson, J. Skalny, Study of the dissolution and electrokinetic behavior of tricalcium aluminate, in: Hydrosols and Rheology, Elsevier, 1976, pp. 211-223.
[9] J. Skalny, M. Tadros, Retardation of tricalcium aluminate hydration by sulfates, Journal of the American Ceramic Society, 60 (1977) 174-175.
[10] H. Minard, S. Garrault, L. Regnaud, A. Nonat, Mechanisms and parameters controlling the tricalcium aluminate reactivity in the presence of gypsum, Cement and Concrete Research, 37 (2007) 1418-1426.
[11] R.J. Myers, G. Geng, E.D. Rodriguez, P. da Rosa, A.P. Kirchheim, P.J.M. Monteiro, Solution chemistry of cubic and orthorhombic tricalcium aluminate hydration, Cement and Concrete Research, 100 (2017) 176-185.
[12] R.J. Myers, G. Geng, J. Li, E.D. Rodríguez, J. Ha, P. Kidkhunthod, G. Sposito, L.N. Lammers, A.P. Kirchheim, P.J. Monteiro, Role of adsorption phenomena in cubic tricalcium aluminate dissolution, Langmuir, 33 (2017) 45-55.
[13] S. Joseph, J. Skibsted, Ö. Cizer, A quantitative study of the C3A hydration, Cement and Concrete Research, 115 (2019) 145-159.

[14] X. Liu, P. Feng, C. Lyu, S. Ye, The role of sulfate ions in tricalcium aluminate hydration: New insights, Cement and Concrete Research, 130 (2020).
[15] S. Ye, P. Feng, Y. Liu, J. Liu, J.W. Bullard, Dissolution and early hydration of tricalcium aluminate in aqueous sulfate solutions, Cement and Concrete Research, 137 (2020).
[16] A.S. Brand, S.B. Feldman, P.E. Stutzman, A.V. Ievlev, M. Lorenz, D.C. Pagan, S. Nair, J.M. Gorham, J.W. Bullard, Dissolution and initial hydration behavior of tricalcium aluminate in low activity sulfate solutions, Cement and Concrete Research, 130 (2020).
[17] R.D. Shannon, Revised effective ionic radii and systematic studies of interatomic distances in halides and chalcogenides, Acta Cryst A, 32 (1976) 751-767.
[18] F. Guo, S. Al-Saadi, R.S. Raman, X. Zhao, Durability of fiber reinforced polymer (FRP) in simulated seawater sea sand concrete (SWSSC) environment, Corrosion Science, 141 (2018) 1-13.
[19] Z. Wang, X.-L. Zhao, G. Xian, G. Wu, R.S. Raman, S. Al-Saadi, A. Haque, Long-term durability of basalt-and glass-fibre reinforced polymer (BFRP/GFRP) bars in seawater and sea sand concrete environment, Construction and Building Materials, 139 (2017) 467-489.
[20] J. Xiao, C. Qiang, A. Nanni, K. Zhang, Use of sea-sand and seawater in concrete construction: Current status and future opportunities, Construction and Building Materials, 155 (2017) 1101-1111.
[21] M.M. Islam, M.S. Islam, M. Al-Amin, M.M. Islam, Suitability of sea water on curing and compressive strength of structural concrete, Journal of Civil Engineering, 40 (2012) 37-45.
[22] P. Li, W. Li, T. Yu, F. Qu, V.W. Tam, Investigation on early-age hydration, mechanical properties and microstructure of seawater sea sand cement mortar, Construction and Building Materials, 249 (2020) 118776.

[23] H.F. Taylor, Cement Chemistry, 2 (1997) 19-22.
[24] I. Maki, Nature of the prismatic dark interstitial material in Portland cement clinker, Cement and Concrete Research, 3 (1973) 295-313.
[25] A. Kirchheim, D. Dal Molin, P. Fischer, A.-H. Emwas, J.L. Provis, P.J.M. Monteiro, Real-time high-resolution X-ray imaging and nuclear magnetic resonance study of the hydration of pure and Na-doped C3A in the presence of sulfates, Inorganic chemistry, 50 (2011) 1203-1212.
[26] A. Boikova, A. Domanskii, V. Paramonova, G. Stavitskaya, V. Nikushchenko, The influence of sodium oxide on the structure and properties of tricalcium aluminate, Cement and Concrete Research, 7 (1977) 483-491.
[27] A. Kirchheim, V. Fernàndez-Altable, P. Monteiro, D. Dal Molin, I. Casanova, Analysis of cubic and orthorhombic C 3 A hydration in presence of gypsum and lime, Journal of materials science, 44 (2009) 2038-2045.
[28] D. Stephan, S. Wistuba, Crystal structure refinement and hydration behaviour of doped tricalcium aluminate, Cement and Concrete Research, 36 (2006) 2011-2020.
[29] R. Yang, J.H. Sharp, Hydration characteristics of Portland cement after heat curing: I, degree of hydration of the anhydrous cement phases, Journal of the American Ceramic Society, 84 (2001) 608-614.
[30] D. Jansen, F. Goetz-Neunhoeffer, B. Lothenbach, J. Neubauer, The early hydration of Ordinary Portland Cement (OPC): An approach comparing measured heat flow with calculated heat flow from QXRD, Cement and Concrete Research, 42 (2012) 134-138.
[31] S. Joseph, R. Snellings, Ö. Cizer, Activation of Portland cement blended with high volume of fly ash using Na2SO4, Cement and Concrete Composites, 104 (2019) 103417.
[32] D. Jansen, J. Neubauer, F. Goetz-Neunhoeffer, R. Haerzschel, W.-D. Hergeth, Change in reaction kinetics of a Portland cement caused by a superplasticizer—Calculation of heat flow curves from XRD data, Cement and Concrete Research, 42 (2012) 327-332.
[33] J. Nehring, J. Neubauer, S. Berger, F. Goetz-Neunhoeffer, Acceleration of OPC by CAC in binary and ternary systems: The role of pore solution chemistry, Cement and Concrete Research, 107 (2018) 264-274.
[34] G. Le Saoût, V. Kocaba, K. Scrivener, Application of the Rietveld method to the analysis of anhydrous cement, Cement and Concrete Research, 41 (2011) 133-148.
[35] O. Linderoth, L. Wadsö, D. Jansen, Long-term cement hydration studies with isothermal calorimetry, Cement and Concrete Research, 141 (2021) 106344.

[36] A. Standard, D1141-98: Standard Practice for the Preparation of Substitute Ocean Water, ASTM International, West Conshohocken, (2013).
[37] K. Scrivener, R. Snellings, B. Lothenbach, A practical guide to microstructural analysis of cementitious materials, Crc Press, 2018.
[38] W. Hummel, U. Berner, E. Curti, F. Pearson, T. Thoenen, Nagra/PSI chemical thermodynamic data base 01/01, Radiochimica Acta, 90 (2002) 805-813.
[39] B. Lothenbach, G. Le Saout, E. Gallucci, K. Scrivener, Influence of limestone on the hydration of Portland cements, Cement and Concrete Research, 38 (2008) 848-860.

[40] B. Lothenbach, T. Matschei, G. Möschner, F.P. Glasser, Thermodynamic modelling of the effect of temperature on the hydration and porosity of Portland cement, Cement and Concrete Research, 38 (2008) 1-18.

[41] B. Lothenbach, D.A. Kulik, T. Matschei, M. Balonis, L. Baquerizo, B. Dilnesa, G.D. Miron, R.J. Myers, Cemdata18: A chemical thermodynamic database for hydrated Portland cements and alkali-activated materials, Cement and Concrete Research, 115 (2019) 472-506.
[42] N. Chitvoranund, F. Winnefeld, C.W. Hargis, S. Sinthupinyo, B. Lothenbach, Synthesis and hydration of alite-calcium sulfoaluminate cement, Advances in Cement Research, 29 (2017) 101-111.
[43] P.G. Gottschalk, J.R. Dunn, The five-parameter logistic: a characterization and comparison with the four-parameter logistic, Analytical biochemistry, 343 (2005) 54-65.
[44] P. Parthasarathy, A. Hanif, H. Shao, Z. Li, Microstructural and morphological studies of ordinary portland cement paste and fly ash based geopolymer in the presence of chloride ions, Construction Materials and Systems, (2017) 623-631.
[45] H. Hirao, K. Yamada, H. Takahashi, H. Zibara, Chloride binding of cement estimated by binding isotherms of hydrates, Journal of Advanced Concrete Technology, 3 (2005) 77-84.
[46] M. Frias, S. Goñi, R. García, R. Vigil de La Villa, Seawater effect on durability of ternary cements. Synergy of chloride and sulphate ions, Composites Part B: Engineering, 46 (2013) 173-178.
[47] R. Talero, L. Trusilewicz, Morphological Differentiation and Crystal Growth Form of Friedel's Salt Originated from Pozzolan and Portland Cement, Industrial & Engineering Chemistry Research, (2012).
[48] A. Suryavanshi, J. Scantlebury, S. Lyon, Mechanism of Friedel's salt formation in cements rich in tri-calcium aluminate, Cement and Concrete Research, 26 (1996) 717-727.
[49] J.-P. Rapin, G. Renaudin, E. Elkaim, M. Francois, Structural transition of Friedel's salt 3CaO· Al2O3· CaCl2· 10H2O studied by synchrotron powder diffraction, Cement and Concrete Research, 32 (2002) 513-519.
[50] R. Allmann, Refinement of the hybrid layer structure $[Ca_2Al\ (OH)_6]^+[1/2SO_4\ .\ 3H_2O]^-$, (1977).
[51] M. François, G. Renaudin, O. Evrard, A cementitious compound with composition 3CaO. Al2O3. CaCO3. 11H2O, Acta Crystallographica Section C: Crystal Structure Communications, 54 (1998) 1214-1217.